Effective equations for anisotropic glioma spread with proliferation: a multiscale approach

Christian Engwer, Alexander Hunt, Christina Surulescu

Tuesday 14th October, 2014

Abstract

Glioma is a common type of primary brain tumor, with a strongly invasive potential, often exhibiting nonuniform, highly irregular growth. This makes it difficult to assess the degree of extent of the tumor, hence bringing about a supplementary challenge for the treatment. It is therefore necessary to understand the migratory behavior of glioma in greater detail. In this paper we propose a multiscale model for glioma growth and migration. Our model couples the microscale dynamics (reduced to the binding of surface receptors to the surrounding tissue) with a kinetic transport equation for the cell density on the mesoscopic level of individual cells. On the latter scale we also include the proliferation of tumor cells via effects of interaction with the tissue. An adequate parabolic scaling yields a convection-diffusion-reaction equation, for which the coefficients can be explicitly determined from the information about the tissue obtained by diffusion tensor imaging. Numerical simulations relying on DTI measurements confirm the biological findings that glioma spreads along white matter tracts.

1 Introduction

Tumor migration and proliferation are two of the most injurious features of cancer, as they happen in detriment of normal tissue. Therefore, the current therapy strategies aim at stopping or at least slowing down these processes. For this in turn, a thorough understanding of the involved phenomena is required. In the last decades mathematical modeling in combination with qualitative and quantitative biological knowledge has become a valuable tool for shading light on many biochemical events involved in cancer development, allowing to make predictions about the evolution of the investigated processes, suggest new experimental settings or even improve therapy approaches.

The invasion of tumor cells into healthy tissue is a highly complex process involving several levels, from the microscopic, intracellular through the intercellular and up to the macroscopic level of a cell population [26]. Most of the events taking place on the various scales are still not completely understood and are part of ongoing research [21]. Mathematical models - simplified to account only for the main features of the invasion process - aim at facilitating reliable information about the tumor in order to provide the optimal therapy. In the present paper we focus on predicting the migratory patterns of glioma, thereby paying particular attention to both cell dispersal along anisotropic structures of the brain and to proliferation.

Gliomas are tumors arising from glia cells. The most common and most aggressive type of primary brain tumour, *glioblastoma multiforme*, has a poor prognosis. The prevailing therapy is surgery, but the tumor is usually infiltrative, which makes complete resection difficult. Radiotherapy (possibly after or concurrent to chemotherapy) can be used to improve the treatment outcome, but it needs, too, informations about the (often very diffuse) shape of the astrocytoma to be irradiated. It is believed that the observed fingering patterns and fibrillar difffusion [13, 16, 23, 40] are due to the glioma following white matter tracts [15, 24, 25] made up of neuron bundles.

Diffusion tensor imaging (DTI) is a common radiological method for tumor diagnosis [46]. It is able to extract neural tract directional information from the measurements of anisotropic diffusion of water molecules in the brain tissue, as the latter is more effective along the aligned fibers than orthogonally to them. This means that the measured rate of diffusion will vary depending on the respective direction. For more details concerning DTI we refer to [3, 17, 48] and for their use in connection to mathematical models for glioma spread we refer to [12, 18, 19, 28, 33, 35, 42]. Most of the mathematical approaches developed so far for this problem are dealing with the macroscopic scale of the tumor and use reaction-diffusion equations (possibly with space and time dependent diffusion coefficients, or accounting for the

interaction with the surrounding tissue by letting the diffusion coefficient be proportional to the water diffusion tensor assessed by DTI) to characterize the glioma density [9, 11, 33, 35, 47, 51]. More advanced settings [28, 42] do not assume the form of the macroscopic equation and its coefficients, but deduce them from a more detailed modeling on the mesoscale of individual cells, on which they set a kinetic transport equation for the density of glioma depending not only on time and space, but also on the velocity of cells. A scaling argument allows then to deduce the macroscopic equation for the population density of cancer cells. While all these models are set on a single (macroscopic or mesoscopic) scale, the latter approach has been recently extended in [18, 19] to a multiscale framework accounting for the subcellular (microlevel) dynamics and connecting it to the mesoscopic evolution of glioma density. An adequate scaling led again to the population level dynamics explicitly carrying the subcellular level information and introducing a supplementary (haptotactic) drift in the macroscale behavior of the tumor. In the present note we retake the modeling approach in [18, 19] and pay particular attention to the description of cell proliferation. Usually, it is realized by a simple choice of the source term (e.g., logistic, Gompertzian, exponential, etc.) on the macroscopic level, which is, again, an assumption inducing supplementary uncertainties in the model and restraining its versatility. This issue has been addressed in [19], where the cell proliferation was characterized relying on the "go-or-grow" hypothesis stating that cancer cells can either move or proliferate [8, 24, 29]. Thereby, the mesolevel transitions between moving and resting regimes played an essential role. As in [18, 28, 42], a parabolic scaling allowed to pass to the macrolevel formulation, in which the logistic growth is a particular case for the description of the source term. Here we propose a new way of modeling proliferation, without necessarily following the "go-or-grow" assumption. Instead, we use cell-tissue interactions to include the proliferation on the mesoscale via microscale dynamics.

The paper is structured as follows: in the next section we introduce our modeling approach. Section 3 deals with the macroscopic scaling, leading to the population dynamics, whose well posedness is addressed as well. The choice of the model parameters for the numerical simulations is motivated in section 4. Section 5 provides the numerical results illustrating the behavior of the glioma density characterized with the macroscopic equation deduced in section 3. Finally, in section 6 we discuss on the performance and the perspectives of our model.

2 Model set up

Our model setting involves two different scales: On the *microscale* it accounts for processes taking place on the subcellular level. Here these reduce to the binding of cell surface receptors (integrins) to unsoluble ligands in the tumor environment and the corresponding mass action kinetics are characterized by an ordinary differential equation (ODE) written for the concentration of bound integrins. The *mesoscale* accounts for the behavior of individual cells and their interactions with the underlying (anisotropic) tissue.

Integrins are heterodimeric transmembrane surface proteins involved -upon activation- in several signaling pathways relevant for glioma behavior, including proliferation, motility, invasion, survival [30, 32, 37]. In our model we regard integrin activation (binding to tissue) as the onset of proliferation and reorientation. The binding dynamics is characterized with the following simple ODE:

$$\dot{y} = k^+(R_0 - y)A - k^- y =: G(y, Q), \tag{1}$$

where y represents the concentration of bound integrins, R_0 denotes the total amount of receptors on the cell (we assume it is conserved), and the constants k^+ and k^- denote the reaction rates for the reversible binding of integrins to the tissue fibres. The macroscopic quantity Q represents the volume fraction of tissue (including ECM and brain fibers), see [18, 19].

On the mesoscale we use a kinetic transport equation to describe the behavior of the glioma density in the form of a density function $p(t, \mathbf{x}, \mathbf{v}, y)$ depending on time t, position $\mathbf{x} \in \mathbb{R}^n$, velocity $\mathbf{v} \in V \subset \mathbb{R}^n$, and internal state[1] $y \in Y \subset \mathbb{R}$. In the absence of proliferation, this equation takes the form

$$\partial_t p + \nabla_{\mathbf{x}} \cdot (\mathbf{v}p) + \partial_y(G(y, Q)p) = \mathcal{L}[\lambda]p, \tag{2}$$

where $\mathcal{L}[\lambda]p := -\lambda(y)p + \lambda(y) \int_V K(\mathbf{x}, \mathbf{v})p(\mathbf{v}')d\mathbf{v}'$ denotes the turning operator modeling the reorientations of cells due to contact guidance by tissue. Thereby, $\lambda(y)$ is the turning rate of cells, depending as in [18, 19] on the amount of bound integrins, and K is the turning kernel carrying the tissue influence. Here it is assumed to take the particular form $K(\mathbf{x}, \mathbf{v}) = \frac{q(\mathbf{x}, \hat{\mathbf{v}})}{\omega}$, where $\hat{\mathbf{v}}$ is the normalized velocity, $q(\mathbf{x}, \hat{\mathbf{v}})$ is the directional distribution of tissue fibers[2], and $\omega = \int_V q(\hat{\mathbf{v}})d\mathbf{v} = s^{n-1}$ is a scaling constant making K

[1] we will use throughout this paper the slightly abusive formulation "internal state" to refer to the bound integrins

[2] hence we also assume these fibers to be undirected

a genuine probability kernel.

As it is difficult to solve numerically the above equations and since the informations about the tumor are assessed on the level of organs and tissue, we aim at deducing a macroscopic equation for the behavior of the glioma population. This amounts to providing an adequate moment closure for the macroscopic scaling. Here we use an ad-hoc closure, assuming that the subcellular dynamics is very fast, hence y is close to the steady state y^* of (1). Following [18, 19], we introduce a new internal variable $z := y^* - y$ measuring deviations from this steady state. This transforms equation (2) into

$$\partial_t p + \mathbf{v} \cdot \nabla p + \partial_z \left(\left(-(k^+ Q + k^-) z + f'(Q) \mathbf{v} \cdot \nabla Q \right) p \right) = \mathcal{L}[\lambda_0] p + \mathcal{L}[\lambda_1] z p, \tag{3}$$

where

$$f(Q(\mathbf{x})) = \frac{k^+ Q(\mathbf{x}) R_0}{k^+ Q(\mathbf{x}) + k^-} \tag{4}$$

and we chose $\lambda(z) = \lambda_0 - \lambda_1 z \geq 0$, with λ_0 and λ_1 some positive constants [3].

Next we want to model cell proliferation. This was done in [19] by making use of the "go-or-grow" dichotomy, considering two subpopulations of cancer cells: moving and resting (i.e., proliferating), respectively. The transitions between these populations along with supplementary source and decay terms characterized their dynamics. While the "go-or-grow" hypothesis has been endorsed by many studies, there are, however, quite a few works, too, providing evidence of proliferation not being deferred for migration (see e.g., [14, 22, 41, 50]), thus preserving its controversial character. In order to avoid such issues we renounce the "go-or-grow" conjecture and try instead to model proliferation just as an effect of cell-tissue interactions (via integrin binding), as announced above.

A way to include proliferation on the mesoscale is to consider a source term of the form

$$\mathcal{P}(p) = \mu\left(\mathbf{x}, \bar{p}, \mathbf{v}\right) \int_Z \chi(\mathbf{x}, z, z') p(t, \mathbf{x}, \mathbf{v}, z') Q(\mathbf{x}) \, dz', \tag{5}$$

where $\bar{p}(t, \mathbf{x}) = \int_V \int_Z p(t, \mathbf{x}, \mathbf{v}, z) \, d\mathbf{v} \, dz$ denotes the macroscopic cell density on which the growth rate μ depends. Thereby, the domain for the internal dynamics is $Z \subseteq [y^* - R_0, y^*]$. The integral operator in (5) involves a kernel χ characterizing the transition from the state z' to the state z during a proliferative action. We do not require χ to be symmetric in the second and third variable nor state any mean value conditions. So this term is rather general, but we will assume the nonlinear operator $\mathcal{P}$ to be uniformly bounded in the L^2 norm. This assumption is reasonable, as space constraints impose bounds on the cell division. The form (5) is motivated by the so-called proliferative interactions in the kinetic theory of active particles (KTAP) framework introduced by Bellomo [6, 7]. Such interaction is modelled here by the product between the mesoscopic density p of tumor cells and the (macroscopic) volume fraction of tissue Q. As mentioned above, we see the cell-tissue interactions (expressed on the microscale by integrin binding) as the onset of proliferation, whence the dependency of χ on z. The proliferation rate μ is assumed to be limited, e.g., by the local competition of tumor cells. A couple of concrete forms will be given in Subsection 4.3. As previously in [19], we ignore cell-cell interactions.

Then our kinetic transport equation on the mesoscale becomes

$$\partial_t p + \nabla \cdot (\mathbf{v} p) - \partial_z (((k^+ Q + k^-) z - f'(Q) \mathbf{v} \cdot \nabla Q) p) = \mathcal{L}[\lambda_0] p - \mathcal{L}[\lambda_1] z p + \mathcal{P}(p). \tag{6}$$

Remark 2.1 *Equation* (6) *aligns to the setting in [34, 38], and the global existence of a unique solution can be proved as in [38], provided μ satisfies an appropriate growth condition w.r.t. its third argument.*

3 Macroscopic scaling

In this section we perform a parabolic scaling in order to convert (6) to a macroscopic equation for the cell population density $\bar{p}(t, \mathbf{x})$, hence reducing the dimension of the phase space. This is particularly useful for the subsequent numerical simulations, as it is hardly possible to measure initial values with respect to the speed $\mathbf{v}$ or the deviation z from the steady state of bounded receptors.

[3] this choice corresponds to the observation that the cell turning rate increases with the amount of bound integrins

Define the variables

$$m(t,\mathbf{x},\mathbf{v}) = \int_Z p(t,\mathbf{x},\mathbf{v},z)\ dz \qquad M(t,\mathbf{x}) = \int_V m(t,\mathbf{x},\mathbf{v})\ d\mathbf{v} = \bar{p}(t,\mathbf{x})$$
$$m^z(t,\mathbf{x},\mathbf{v}) = \int_Z zp(t,\mathbf{x},\mathbf{v},z)\ dz \qquad M^z(t,\mathbf{x}) = \int_V m^z(t,\mathbf{x},\mathbf{v})\ d\mathbf{v}$$

and assume the data to be compactly supported in the $(\mathbf{x},\mathbf{v},z)$ space, which justifies the subsequent calculations.
As in [18, 19], integrate (6) w.r.t. z. Then multiply (6) by z and integrate again w.r.t. z. The higher (starting from the second) order moments of p w.r.t. z can be neglected due to our assumption of small deviations from the steady state of (1). These steps lead to the equations

$$\begin{aligned}\partial_t m + \nabla_{\mathbf{x}}\cdot(\mathbf{v}m) &= -\lambda_0 m + \lambda_1 m^z + \lambda_0\frac{q}{\omega}M - \lambda_1\frac{q}{\omega}M^z \\ &\quad + \mu(\mathbf{x},M,\mathbf{v})\int_Z\int_Z \chi(\mathbf{x},z,z')p(z')Q(\mathbf{x})\ dz'\ dz \\ \partial_t m^z + \nabla_{\mathbf{x}}\cdot(\mathbf{v}m^z) &= -(k^+Q+k^-)m^z + f'(Q)\mathbf{v}\cdot\nabla Q m - \lambda_0 m^z + \lambda_0\frac{q}{\omega}M^z \\ &\quad + \mu(\mathbf{x},M,\mathbf{v})\int_Z\int_Z z\chi(\mathbf{x},z,z')p(z')Q(\mathbf{x})\ dz'\ dz.\end{aligned}$$

3.1 Formal parabolic limit

Now use $\hat{t} = \epsilon^2 t$, $\hat{\mathbf{x}} = \epsilon\mathbf{x}$ to rescale the time and space variables. Moreover, the proliferation rate is rescaled with ϵ^2 to let it act on the correct new time scale. After dropping the hats on the new variables for simplicity of writing we obtain

$$\begin{aligned}\epsilon^2\partial_t m + \epsilon\nabla\cdot(\mathbf{v}m) &= -\lambda_0 m + \lambda_1 m^z + \lambda_0\frac{q}{\omega}M - \lambda_1\frac{q}{\omega}M^z \\ &\quad + \epsilon^2\mu(\mathbf{x},M,\mathbf{v})\int_Z\int_Z \chi(\mathbf{x},z,z')p(z')Q(\mathbf{x})\ dz'\ dz \qquad (7) \\ \epsilon^2\partial_t m^z + \epsilon\nabla\cdot(\mathbf{v}m^z) &= -(k^+Q+k^-+\lambda_0)m^z + \lambda_0\frac{q}{\omega}M^z + \epsilon f'(Q)\mathbf{v}\cdot\nabla Q m \\ &\quad + \epsilon^2\mu(\mathbf{x},M,\mathbf{v})\int_Z\int_Z z\chi(\mathbf{x},z,z')p(z')Q(\mathbf{x})\ dz'\ dz. \qquad (8)\end{aligned}$$

With the Hilbert expansions

$$m = \sum_{k=0}^{\infty}\epsilon^k m_k \qquad M = \sum_{k=0}^{\infty}\epsilon^k M_k$$
$$m^z = \sum_{k=0}^{\infty}\epsilon^k m_k^z \qquad M^z = \sum_{k=0}^{\infty}\epsilon^k M_k^z$$

we obtain by collecting the coefficients of the powers of ϵ:
ϵ^0 :

$$\begin{aligned}0 &= -\lambda_0 m_0 + \lambda_1 m_0^z + \lambda_0\frac{q}{\omega}M_0 - \lambda_1\frac{q}{\omega}M_0^z \\ 0 &= -(\lambda_0 + k^+Q + k^-)m_0^z + \lambda_0\frac{q}{\omega}M_0^z\end{aligned}$$

ϵ^1 :

$$\begin{aligned}\nabla\cdot(\mathbf{v}m_0) &= -\lambda_0 m_1 + \lambda_1 m_1^z + \lambda_0\frac{q}{\omega}M_1 - \lambda_1\frac{q}{\omega}M_1^z \\ \nabla\cdot(\mathbf{v}m_0^z) &= -(\lambda_0 + k^+Q + k^-)m_1^z + \lambda_0\frac{q}{\omega}M_1^z + f'(Q)\nabla\cdot(\mathbf{v}Q)m_0\end{aligned}$$

ϵ^2 :

$$\partial_t m_0 + \nabla \cdot (\mathbf{v} m_1) = -\lambda_0 m_2 + \lambda_1 m_2^z + \lambda_0 \frac{q}{\omega} M_2 - \lambda_1 \frac{q}{\omega} M_2^z + \mu(\mathbf{x}, M, \mathbf{v}) \int_Z \int_Z \chi(\mathbf{x}, z, z') p(z') Q(\mathbf{x}) dz' dz.$$

We still have to specify the growth rate μ and the integral kernel χ in order to obtain a closed form equation. To this aim we expand μ about M_0:

$$\mu(\mathbf{x}, M, \mathbf{v}) = \mu(\mathbf{x}, M_0, \mathbf{v}) + \partial_M \mu(\mathbf{x}, M_0, \mathbf{v})(M - M_0) + \mathcal{O}(|M - M_0|^2)$$

Recognizing that $M - M_0 = \sum_{i=1}^{\infty} \epsilon^i M_i = \mathcal{O}(\epsilon)$, the equation involving the second powers of ϵ reads as:

$$\partial_t m_0 + \nabla \cdot (\mathbf{v} m_1) = -\lambda_0 m_2 + \lambda_1 m_2^z + \lambda_0 \frac{q}{\omega} M_2 - \lambda_1 \frac{q}{\omega} M_2^z + \mu(\mathbf{x}, M_0, \mathbf{v}) Q(\mathbf{x}) \int_Z \int_Z \chi(\mathbf{x}, z, z') p(z') dz' dz.$$

We assume $\chi(\mathbf{x}, z, z')$ to be a probability kernel with respect to z for all $(\mathbf{x}, z')$, meaning that there is some probability distribution independent of the space variable and the integrin bindings describing the state of the cell previous to a proliferation event. Then we have

$$\int_Z \int_Z \chi(\mathbf{x}, z, z') p(z') dz' \, dz = \int_Z p(z') \, dz' = m_0 + \mathcal{O}(\epsilon),$$

which leads to the closed form ϵ^2 equation

$$\partial_t m_0 + \nabla \cdot (\mathbf{v} m_1) = -\lambda_0 m_2 + \lambda_1 m_2^z + \lambda_0 \frac{q}{\omega} M_2 - \lambda_1 \frac{q}{\omega} M_2^z + Q(\mathbf{x}) \mu(\mathbf{x}, M_0, \mathbf{v}) m_0. \tag{9}$$

Now we can compute the quantities involved in the system of equations. By integrating the ϵ^0 equations with respect to $\mathbf{v}$, it immediately follows that $M_0^z = 0$, so by the second equation $m_0^z = 0$. Inserting this into the first equation yields $m_0 = \frac{q}{\omega} M_0$.
Now integrating the ϵ^1 equations with respect to $\mathbf{v}$ and recalling the assumption of undirected fibers we obtain the following auxiliary system:

$$\nabla \cdot \left(\int_V \mathbf{v} \frac{q}{\omega} M_0 \, d\mathbf{v} \right) = 0$$

$$0 = -(k^+ Q + k^-) M_1^z + f'(Q) \nabla Q \cdot \int_V \mathbf{v} \frac{q}{\omega} M_0 \, d\mathbf{v}.$$

The second equation simplifies to $M_1^z = 0$. Then we can compute m_1^z as

$$m_1^z = (k^+ Q + k^- + \lambda_0)^{-1} (f'(Q) \nabla \cdot (\mathbf{v} Q) m_0).$$

Now we use the properties of the compact Hilbert-Schmidt operator $\mathcal{L}[\lambda_0](m_1) = -\lambda_0 m_1 + \lambda_0 \frac{q}{\omega} M_1$ defined on the weighted space $L_q^2(V)$, with weight function $q^{-1}(\hat{\mathbf{v}})$. For this operator we can find on $\langle q \rangle^\perp$ a pseudoinverse, and get $M_1 = 0$, hence

$$m_1 = -\lambda_0^{-1} \left(\nabla \cdot \left(\mathbf{v} \frac{q}{\omega} M_0 \right) - \lambda_1 (k^+ Q + k^- + \lambda_0)^{-1} f'(Q) \mathbf{v} \cdot \nabla Q \frac{q}{\omega} M_0 \right).$$

For more details we refer to [27, 18].

To summarize, we computed the following quantities:

$$m_0 = \frac{q}{\omega} M_0 \tag{10}$$

$$m_0^z = 0 \tag{11}$$

$$M_0^z = 0 \tag{12}$$

$$m_1 = -\frac{1}{\lambda_0} \left(\nabla \cdot \left(\mathbf{v} \frac{q}{\omega} M_0 \right) - \lambda_1 m_1^z \right) \tag{13}$$

$$m_1^z = \frac{f'(Q)}{k^+ Q + k^- + \lambda_0} \nabla \cdot \left(\mathbf{v} Q \frac{q}{\omega} \right) M_0 \tag{14}$$

$$M_1 = 0 \tag{15}$$

$$M_1^z = 0. \tag{16}$$

Now integrating the above ϵ^2 equation (9) with respect to $\mathbf{v}$ yields

$$\int_V \Big(\partial_t(\frac{q}{\omega}M_0) + \nabla\cdot(\mathbf{v}m_1)\Big)\, d\mathbf{v} = Q(\mathbf{x})\int_V \mu(\mathbf{x}, M_0, \mathbf{v})m_0\, d\mathbf{v},$$

which with the functions calculated above leads to the macroscopic equation

$$\partial_t M_0 - \nabla\nabla : (\mathbb{D}_T M_0) + \nabla\cdot(g(Q(\mathbf{x}))\mathbb{D}_T\nabla Q M_0) = Q(\mathbf{x})\mu(\mathbf{x}, M_0)M_0, \tag{17}$$

where we assumed μ not to depend on $\mathbf{v}$ explicitly. The function $g(Q(\mathbf{x})) := \lambda_1(k^+Q+k^-+\lambda_0)^{-1}f'(Q(\mathbf{x}))$ carries the information from the subcellular dynamics of receptor binding and

$$\mathbb{D}_T(\mathbf{x}) = \frac{1}{\lambda_0\omega}\int_V q\mathbf{v}\otimes\mathbf{v}\, d\mathbf{v} \tag{18}$$

is the tumor diffusion tensor. Equation (17) is a short form of

$$\partial_t M_0 - \nabla\cdot(\mathbb{D}_T(\mathbf{x})\nabla M_0) + \nabla\cdot(g(Q(\mathbf{x}))\mathbb{D}_T(\mathbf{x})\nabla Q(\mathbf{x}) - \mathbf{u}(\mathbf{x}))M_0) = Q(\mathbf{x})\mu(\mathbf{x}, M_0)M_0, \tag{19}$$

with the drift velocity

$$\mathbf{u}(\mathbf{x}) = \frac{1}{\lambda_0\omega}\int_V \mathbf{v}\otimes\mathbf{v}\nabla q\, d\mathbf{v}. \tag{20}$$

3.2 Well-posedness of the macroscopic model

Due to the model complexity we cannot rigorously prove the convergence of the mesoscopic equation (6) to the macroscopic one (17). Thus, it is not offhand clear whether the existence and uniqueness result obtained for (6) carries over to the equation deduced on the macroscale and we have to check whether (17) together with some adequate initial condition is well posed. To this aim we will use the theory of monotone operators and follow [43, 44]. We will consider here the problem on a bounded domain $\Omega\subset\mathbb{R}^3$ with $\partial\Omega\in C^{0,1}$, which then can be extended to the full space $\mathbb{R}^3$.

We consider the following problem:

$$\partial_t w - \nabla\cdot(\mathbb{D}_T\nabla w) + \nabla\cdot(\boldsymbol{\Upsilon}(Q,\mathbb{D}_T)w) - \Gamma(w) = 0 \quad \text{in } [0,T]\times\Omega \tag{21}$$

$$\nabla w\cdot\mathbf{n} = 0 \quad \text{on } [0,T]\times\partial\Omega, \tag{22}$$

$$w(0) = w_0 \quad \text{in } \Omega, \tag{23}$$

with a finite $T>0$ and Ω as above, $\Gamma(w) := Q(\mathbf{x})\mu(\mathbf{x},w)w$, and $\boldsymbol{\Upsilon}(Q,\mathbb{D}_T) := g(Q(\mathbf{x}))\mathbb{D}_T(\mathbf{x})\nabla Q(\mathbf{x}) - \mathbf{u}(\mathbf{x})$.

Set $U := H^1(\Omega)$, $H := L^2(\Omega)$, and $X := L^2(0,T;H^1(\Omega))$. We define for all $w,\zeta\in X$:

$$\langle A_1 w,\zeta\rangle_X := \int_0^T\int_\Omega (\mathbb{D}_T\nabla w - \boldsymbol{\Upsilon}(Q,\mathbb{D}_T)w)\cdot\nabla\zeta\, d\mathbf{x}dt =: \langle Aw,\zeta\rangle_X + \langle\tilde{A}w,\zeta\rangle_X,$$

$$\langle A_2 w,\zeta\rangle_X := -\int_0^T\int_\Omega \Gamma(w)\zeta\, d\mathbf{x}dt.$$

Subsequently we require the continuous function $\Gamma:\mathbb{R}\to\mathbb{R}$ to satisfy the following conditions:

$$|\Gamma(s)| \le C(1+|s|^{r-1}) \quad \text{for some finite } r\ge 1, \tag{24}$$

$$\inf_{s\in\mathbb{R}}\Gamma(s)s > -\infty \tag{25}$$

and the tensor $\mathbb{D}_T(\mathbf{x})$ to be positive definite for a.e. $\mathbf{x}$ and have its smallest eigenvalue larger then some $\alpha>0$. Moreover, $\mathbb{D}_T$ should be in $L^\infty(\Omega)$. [4]

Theorem 3.1 *Let $w_0\in L^2(\Omega)$ and the continuous function $\Gamma:\mathbb{R}\to\mathbb{R}$ satisfy the conditions* (24), (25), *with $1\le r<\frac{10}{3}$. Then there exists a solution w in*

$$W := \{w\in L^2(0,T;H^1(\Omega)) \ :\ w_t\in L^2(0,T;(H^1(\Omega))^*)\}$$

[4] These conditions are actually satisfied by the tumor diffusion tensor obtained via (18) from the DTI data.

of the problem (21)-(23)*, i.e. for all* $\zeta \in C_0^\infty([0,T]\times\Omega)$ *it holds that*

$$\int_0^T \langle \frac{dw(t)}{dt}, \zeta(t)\rangle_{H^1(\Omega)} dt + \int_0^T \int_\Omega (\mathbb{D}_T \nabla w(t) - \boldsymbol{\Upsilon}(Q,\mathbb{D}_T) w(t)) \cdot \nabla\zeta \; d\mathbf{x}dt + \int_0^T \int_\Omega \Gamma(w(t))\zeta(t) \; d\mathbf{x}dt = 0. \tag{26}$$

The proof requires some preliminary results:

Lemma 3.1 *The operator* A_1 *maps* X *into its dual* X^**. The operator* $A : X \to X^*$ *is strictly monotone, coercive, bounded, and continuous. The operator* $\tilde{A} : X \to X^*$ *is continuous and bounded.*

Proof: This is straightforward, due to the properties of $\mathbb{D}_T$ and the concrete form of $\boldsymbol{\Upsilon}(Q,\mathbb{D}_T)$ involving $Q, \mathbb{D}_T$, and the drift velocity $\mathbf{u}$ given in (29).
As $W \subseteq X$, we also have that $A : W \to W^*$ has the properties of $A : X \to X^*$. □

Lemma 3.2 *There exist some constants* $\beta, \delta > 0$ [5] *such that the following coercivity condition holds for the operator* $A_1 : X \to X^*$*:*

$$\langle A_1 w, w\rangle_X \geq \delta \|\nabla w\|^2_{L^2(0,T;L^2(\Omega))} - \gamma \|w\|^2_{L^2(0,T;L^2(\Omega))}. \tag{27}$$

Proof: This is again an easy computation relying on the concrete form of $\boldsymbol{\Upsilon}(Q,\mathbb{D}_T)$ and the fact that Q and $\mathbb{D}_T$ are uniformly bounded. □

Remark 3.1 *Inequality* (27) *differs from the usual coercivity condition. Observe, however, that by denoting* $\omega := e^{-\gamma t} w$ *we obtain an equivalent problem*

$$\partial_t \omega - \nabla\cdot(\mathbb{D}_T \nabla\omega) + \nabla\cdot(\boldsymbol{\Upsilon}(Q,\mathbb{D}_T)\omega) + \gamma\omega - \Gamma(\omega) = 0 \quad \text{in } [0,T]\times\Omega. \tag{28}$$

The operator $\tilde{A}_1$ *defined by*

$$\langle \tilde{A}_1\omega, \zeta\rangle_X := \langle A_1\omega, \zeta\rangle_X + \gamma \int_0^T \int_\Omega \omega\zeta \; d\mathbf{x}dt$$

now satisfies the usual coercivity condition

$$\langle \tilde{A}_1\omega, \omega\rangle_X \geq \delta \|\nabla\omega\|^2_{L^2(0,T;L^2(\Omega))}.$$

In the following we will use equation (28) *and the operators* $\tilde{A}_1$*,* A_2*. Observe that in virtue of Lemma 3.1 the operator* $\tilde{A}_1 : W \to W^*$ *is continuous, strictly monotone, coercive, and bounded.*

Lemma 3.3 *Let* Γ *satisfy* (24) *and* (25)*. If* $r \leq \frac{10}{3}$*, then* A_2 *maps* W *into its dual* W^* *and is bounded. For* $r < \frac{10}{3}$ *the operator* A_2 *is strongly continuous.*

Proof: See Lemma 3.103, Chapter 3 in [43]. □

Lemma 3.4 *Under the above conditions the operator* $\tilde{A}_1 + A_2 : W \to W^*$ *is coercive.*

Proof: See Lemma 3.105, Chapter 3 in [43]. □

Now the proof of Theorem 3.1 follows as in [43], Theorem 3.106, Chapter 3 (see also the remark thereafter) and Section III.4.1. in [44].

Proposition 3.1 *The above solution of the macroscopic problem is unique, provided the function* $\mu(\mathbf{x},\cdot)$ *is Lipschitz continuous.*

Proof: This follows with the usual estimates, by a simple application of Gronwall's inequality and using Lemma 3.2 and Remark 3.1. □

Proposition 3.2 *The solution of the macroscopic problem* (21)-(23) *with* $w_0 \geq 0$ *is nonnegative.*

Proof: Take $\omega = \omega^+ - \omega^-$, $\omega \in W$ and test (28) with ω^-, then apply Gronwall's inequality to deduce $\omega^- = 0$.

□

[5] depending on the L^∞-bound of $\boldsymbol{\Upsilon}(Q,\mathbb{D}_T)$

4 Assessment of parameters and coefficient functions

For the numerical simulation we also have to specify the necessary parameters. We rely on DTI measurements [6]. The preprocessed data include segmentation data, apparent water diffusion tensors, and a brainmask for each voxel of the brain of a healthy adult. All numerical simulations are performed on this particular brain structure, assuming a (superimposed) initial tumor. The DTI measurements provide valuable information about the structure of the main coefficients in the macroscopic equation (17). They allow to explicitly compute the tumor diffusion tensor $\mathbb{D}_T$ in (18) and the drift velocity in (29) with the aid of the water diffusion tensor $\mathbb{D}_W$. Moreover, they also allow to estimate the fiber orientation and the volume fraction Q (see subsections 4.1 and 4.2 below).

4.1 Estimating the fiber orientation

To determine the diffusion coefficient in (19) we need to choose the fiber density q in equation (18) for the tumor diffusion tensor. As in [18, 19] we consider the so-called peanut distribution

$$q(\mathbf{x}, \boldsymbol{\theta}) = \frac{n}{|\mathbb{S}^{n-1}| tr(\mathbb{D}_W(\mathbf{x}))} \boldsymbol{\theta}^T \mathbb{D}_W \boldsymbol{\theta},$$

where $\mathbb{D}_W$ denotes the DTI-measured water diffusion tensor. Then (see [18]) the tumor diffusion tensor in (18) can be computed as

$$\mathbb{D}_T(\mathbf{x}) = \frac{s^2}{\lambda_0(n+2)} \left(I + 2 \frac{\mathbb{D}_W(\mathbf{x})}{tr(\mathbb{D}_W(\mathbf{x}))} \right)$$

and the drift velocity 20 takes the concrete form

$$\mathbf{u}(\mathbf{x}) = \frac{2s^2}{\lambda_0(n+2)} \left(\frac{\nabla \cdot \mathbb{D}_W(\mathbf{x})}{\operatorname{tr} \mathbb{D}_W(\mathbf{x})} - \frac{\mathbb{D}_W(\mathbf{x}) \cdot \nabla \operatorname{tr} \mathbb{D}_{\mathbf{W}}(\mathbf{x})}{(\operatorname{tr} \mathbb{D}_W(\mathbf{x}))^2} \right), \tag{29}$$

where s denotes the average cell speed, which is assumed to be constant. It has also been argued [42] that a bimodal von Mises-Fisher distribution may be more appropriate to model the dependence of q on $\mathbb{D}_W$. In this case q takes the form [39]

$$q(\mathbf{x}, \boldsymbol{\theta}) = \frac{k(\mathbf{x})}{8\pi \sinh(k(\mathbf{x}))} \left(\exp(k(\mathbf{x}) \boldsymbol{\phi} \cdot \boldsymbol{\theta}) + \exp(-k(\mathbf{x}) \boldsymbol{\phi} \cdot \boldsymbol{\theta}) \right), \tag{30}$$

where $k(\mathbf{x}) = \kappa FA(\mathbf{x})$ with the fractional anisotropy FA and a real constant κ to be determined. The vector $\boldsymbol{\phi}$ represents the leading eigenvector of the diffusion tensor for each voxel. The main problem with this choice is the value of κ, as for different choices of it we can obtain more (for large κ) or less (for smaller κ) pronounced anisotropic behavior. Moreover, it is not clear how to measure such parameter in the present context, hence we will not use this distribution for our simulations, except for a comparison between our model and the one using it in [42].

4.2 Estimating the volume fraction of tissue fibers

In previous works [18, 19] the macroscopic quantity Q was chosen to be the fractional anisotropy, which is assessed from measurements. The argumentation was that the volume fraction Q of brain matter should be high where the tissue is strongly aligned. While this seems to be true for highly anisotropic regions, this choice may become problematic in regions consisting of isotropic (non-aligned) and densely packed tissue. This motivates to look for an alternative estimation of this quantity.
The characteristic (diffusion) length l_c is defined as $\sqrt{tr(\mathbb{D}_W) t_c}$ and represents the mean free space in every direction. Hence the space occupied inside a a cube volume V is obtained as $V - l_c^3$, i.e., the maximal volume minus the free space portion. We still need an estimate for the characteristic time t_c and we aim to obtain it from the DTI data. We consider it to be the expected exit time from the volume V of a particle starting in the center and moving randomly according to the DTI diffusion tensor. After a normalization of Q by division with the volume V we get the overall representation $Q(\mathbf{x}) = 1 - \frac{l_c^3(\mathbf{x})}{V}$.

[6] provided by Carsten Wolters (Institute for Biomagnetism and Biosignal Analysis, WWU Münster)

4.3 Selecting the growth rate

There is a large variety of choices which can be made for the growth rate. In the absence of biological data every such choice is arguable and we have to rely on different existing model types. Hence, reasonable choices of μ are

$$\mu_1(M_0) = c_g \left(1 - \frac{M_0}{C_M}\right) \quad \text{or}$$
$$\mu_2(M_0) = -c_g \ln\left(\frac{M_0}{C_M}\right).$$

The former corresponds to logistic growth of a population with carrying capacity C_M; this choice and has been made e.g., in [33, 51]. The other choice μ_2 describes Gompertzian growth, which has been preferred due to better fitting of growth data, especially among avascular tumor growth power law (see e.g. [2] and the references therein). However, it is still lacking a truly fundamental explanation. The best choice of the growth model (also beyond Gompertz vs. logistic) is yet a controversial issue.

4.4 Selecting the remaining constants

The following table specifies the rest of the involved constants:

Parameter	Value	Source
R_0	10^5	[5]
s	$0.21 \cdot 10^{-6} \frac{m}{\mathrm{s}}$	[10]; we used $0.25 \cdot 10^{-6} \frac{m}{\mathrm{s}}$
λ_0	$0.1 \frac{1}{\mathrm{s}}$	[45]
λ_1	$0.01 \frac{1}{\mathrm{s}}$	as in [18]
k^+	$0.1 \frac{1}{\mathrm{s}}$	as in [18], assumed to equal the dettachment rate (or be comparable, to the same order of magnitude)
k^-	$0.1 \frac{1}{\mathrm{s}}$	[36]
c_g	$\approx 8.44 \cdot 10^{-7} \frac{1}{\mathrm{s}} - \approx 1.01 \cdot 10^{-6} \frac{1}{\mathrm{s}}$	estimated as below.
c_M	≈ 1	estimated.

Table 1: Model parameters

For the value of the constant c_g we have either to rely on measurements or estimate it with the aid of the duration of a cell cycle. The first method is widely accepted and used, however it has some shortcomings. For example, the (tumor) volume doubling rate is known by measurements, but this value only gives the visible size (up to 80%) and moreover it is not directly connected to the tumor cell density, hence the error done is twofold. It is known that GBM tumors in particular show a highly migratory behavior and so the moving cells which got far enough from the tumor are not counted. Furthermore, the visible tumor is heterogeneous with respect to its cells and even with respect to their density, making the reliable assessment of c_g via measurements a very difficult task.
The second possibility directly relates to the cell type. We used for the cell cycle duration 205200s, hence about 57 hours - corresponding to the mean cell cycle measured in [31] Then the rate would be $\frac{\ln(2)}{205200\mathrm{s}}$. But this value is not the correct one, because not every cell in a tumor is actively going through its cycle; most of the tumor cells are actually in a quiescent phase, in which they rest and interrupted division, see, e.g., [1]. In [49] the authors estimated the fraction of actively cycling cells between 25% and 30%. This leads to $c_g = \frac{\text{fraction of actively cycling cells}}{\text{duration of a cell cycle}} \cdot \ln 2$.

5 Numerical simulations

We solve the macroscopic equation (19). All involved coefficients are calculated using the octave numerics software. Then the simulation of the PDE is implemented via DUNE [4].
The coefficients $\mathbb{D}_T$ and the drift term are spatially dependent, so we expect regions of the computational domain that are dominated by the diffusion term and others dominated by the drift term. Thus we need numerical methods capable to handle both diffusion dominated and degenerated parabolic equations. Moreover, the selected method has to handle full tensors and should be locally mass conservative.

5.1 Implementation

For the simulation we use a parallel structured quadrilateral mesh as implemented in YaspGrid of DUNE. The cells are chosen in such a way that we have a subset of the voxel mesh given by the DTI dataset we use, so that we can really compute only on the regions of the brain consisting of white and gray brain matter. The segmentation of the brain was given in the dataset. On this mesh we use a symmetric interior penalty discontinuous Galerkin method as implemented in DUNE [4]. The drift term is computed in a continuous fashion as a Raviart-Thomas RT0 approximation and the tumor diffusion tensor is constant over one computational cell. Moreover, to be robust with respect to heterogeneous diffusion, we use weighted jumps in the discretization. More details on the discretization can be found e.g., in [18, 20]. For the time discretization we use an implicit Euler scheme with a step size τ satisfying a CFL-condition near 1. In our case we have selected τ to be about half a day.

5.2 Results for the model (19)

The simulation results for the model (19) performed in a 2D domain representing a single slice of a human brain (from our data sets) are shown in Figure 1 for the logistic growth case (hence with the growth rate $\mu_1(M_0)$) and in Figure 4 for the Gompertzian growth case (with growth rate $\mu_2(M_0)$), respectively. As in [18, 19], notice that the tumor cells follow the anisotropic structure of the brain white matter. Figure 2 shows the structure of the computational brain slice when the volume fraction of tissue fibers is represented by the (arguable) choice of fractional anisotropy as assessed from DTI measurements (left) and by the estimation done in Subsection 4.2 (right).
Our model applied to the case with fractional anisotropy predicts a much faster glioma spread, while the choosing the estimated Q for the volume fraction of tissue fibers shows an enhanced, however more localized growth, as illustrated more clearly in Figure 3.

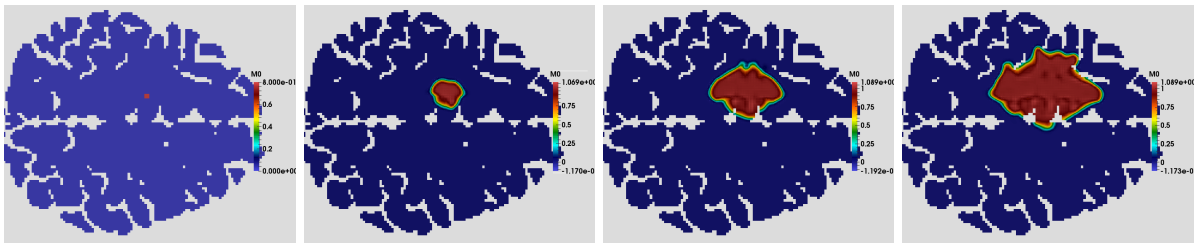

Day 0 Day 200 Day 400 Day 600

(a) Simulation results for (19) with fractional anisotropy and logistic growth

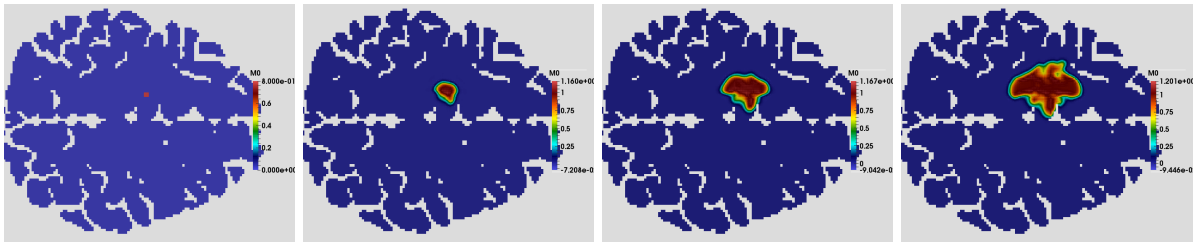

Day 0 Day 200 Day 400 Day 600

(b) Simulation results for (19) with the estimated Q and logistic growth

Figure 1: Simulation results for (19) with growth function μ_1

5.3 Comparison between our new model and previous approaches

Figure 5 illustrates the difference between the solution behavior for the model studied here (describing cell proliferation as in (5)) and the one for model previously introduced in [19] to comply with the "go-or-grow" hypothesis. Observe that the new model predicts a larger extent of tumor spread and the difference between the two models becomes more accentuated with evolving time.
Compared to pure diffusion models as in e.g., [33, 47, 51] involving constant or space-varying diffusion coefficients, our multiscale approach leading to a supplementary drift term predicts a more anisotropic

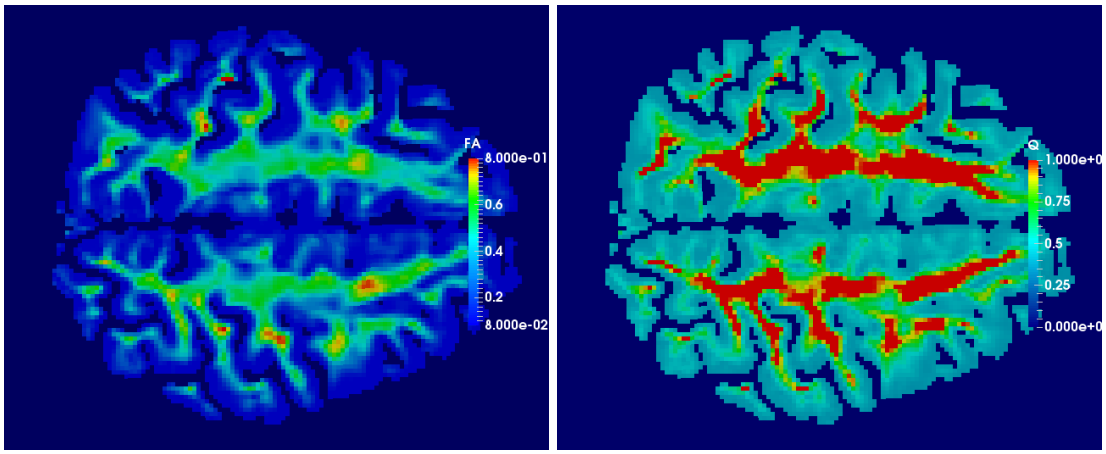

(a) Fractional anisotropy (b) Estimated Q

Figure 2: Fractional anisotropy and the estimated Q in the computational slice.

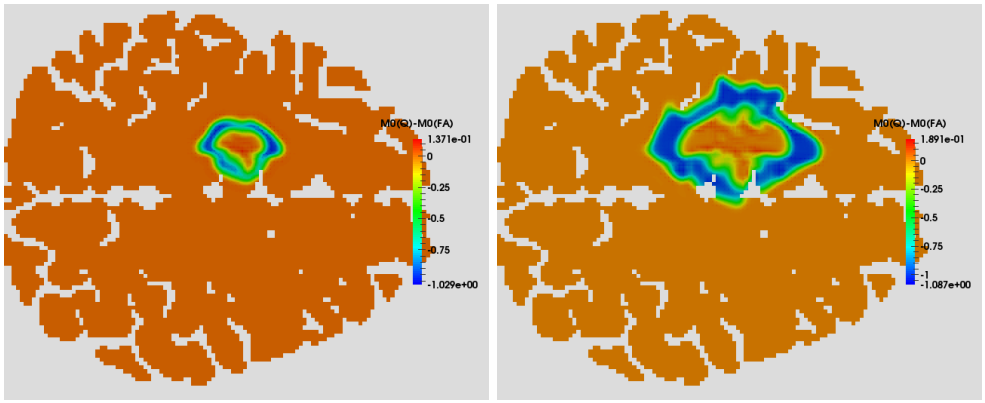

(a) Day 280 (b) Day 560

Figure 3: Difference $M_0(Q) - M_0(FA)$ between the simulation done with the estimated Q and with fractional anisotropy, respectively; logistic growth case.

cancer spread, following the white matter structure. This is in accordance to the findings in [18, 19]. Figure 6 illustrates this difference. Thereby, the pure diffusion model has the form

$$\partial_t M_0 - \nabla \cdot (\mathbb{D}_T(\mathbf{x}) \nabla M_0) = Q(\mathbf{x}) \mu(\mathbf{x}, M_0) M_0.$$

Notice that the above model (although with the diffusion coefficient involving $\mathbb{D}_T$ computed from the DTI data at each space point $\mathbf{x}$) substantially overestimates the tumor growth in the more isotropic brain structure and drastically underestimates glioma invasion at the tumor edges in the anisotropic part. This might lead to a relatively fast tumor recurrence (e.g., after surgery, due to insufficient resection at the invasion front).
A similar comparison between the drift-diffusion model

$$\partial_t M_0 - \nabla\nabla : (\mathbb{D}_T(\mathbf{x}) M_0) = Q(\mathbf{x}) \mu(\mathbf{x}, M_0) M_0$$

deduced in [42] and the multiscale approach in this paper is presented in Figure 7 below. Thereby, following [42] we choose for q the von Mises-Fisher distribution in (30) with the concentration $\kappa(\mathbf{x}) = \kappa$ taking the values $\kappa = 10$, $\kappa = 20$, and the very large value $\kappa = 10^4$. The latter means that the directional distribution of tissue fibers becomes highly concentrated about the angle $\boldsymbol{\theta}$, thus enforcing anisotropic behavior. Notice that neither this choice can capture the strongly anisotropic (finger-like) spread predicted by our model (especially at the invasion fronts), although it performs better than the pure diffusion approach.

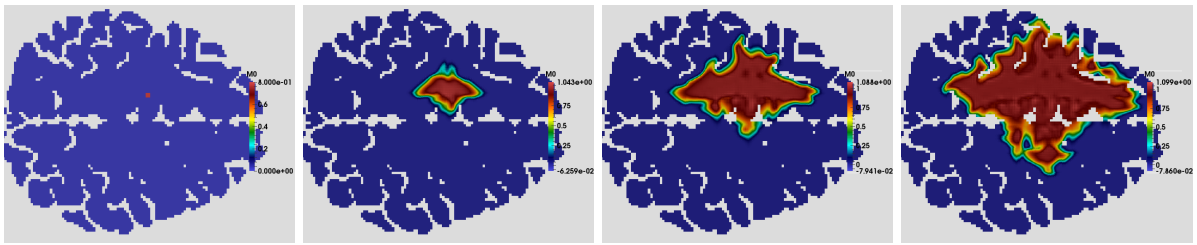

Day 0 Day 100 Day 200 Day 300

(a) Simulation results for (19) with fractional anisotropy and Gompertz growth

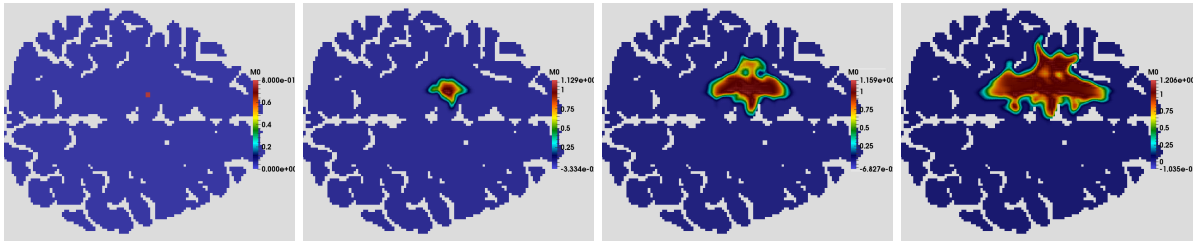

Day 0 Day 100 Day 200 Day 300

(b) Simulation results for (19) with the estimated Q and Gompertz growth

Figure 4: Simulation results for (19) with growth function μ_2.

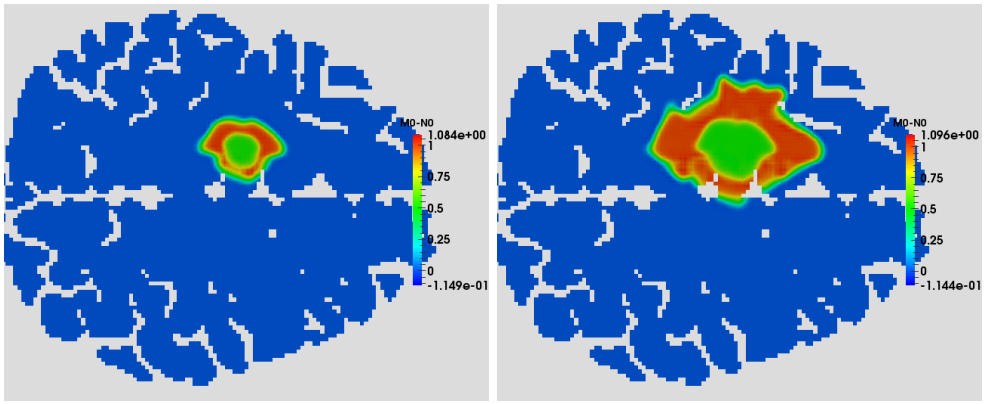

(a) Day 280 (b) Day 560

Figure 5: Difference $M_0 - N_0$ between the solutions to the model with cell proliferation as in (5) and the previous model in [19] relying on the 'go-or-grow' dichotomy. The growth is characterized with the aid of μ_1 in Subsection 4.3.

5.4 Comparison between 2D and 3D

In order to assess possible implications of a supplementary space dimension we also simulated the model (19) in three dimensions. Figure 8 shows top and side views of a couple of snapshots for the tumor evolution. As these simulations are much more expensive than their 2D counterparts we compared the 3D results (more precisely the projection on the corresponding 2D brain slice) with the simulations obtained directly for that particular 2D domain. Figures 9a and 9b show snapshots of the respective tumor evolution. Notice the high resemblance of the results; the projected 3D case exhibits for longer runs a slightly enhanced tumor growth (the difference is of the order of 10^{-2}). This shows that the the less costy 2D simulations are already relevant for conclusions about the glioma behavior.

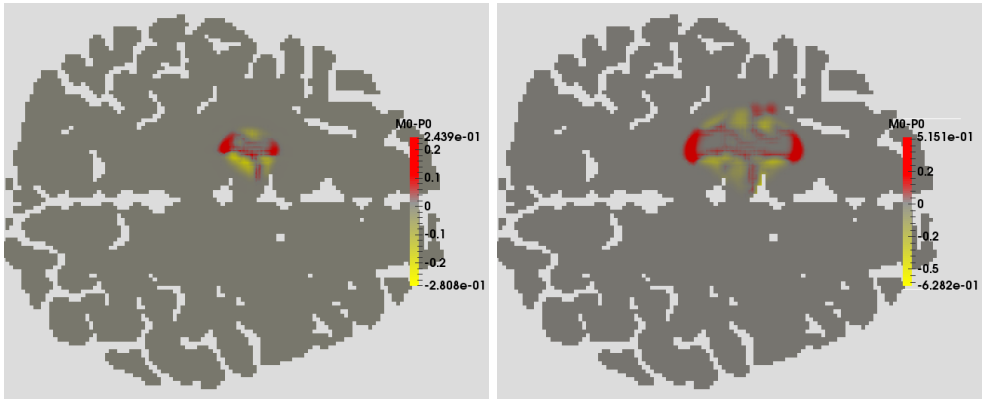

(a) Day 280 (b) Day 560

Figure 6: Difference $M_0 - P_0$ between the solutions obtained by our multiscale approach and the one using a pure diffusion model set directly on the macroscale, respectively.

6 Discussion and outlook

In this work we proposed a multiscale model for glioma invasion accounting for proliferation on the mesoscale. As in [19] this constitutes an extension of previous mathematical models where cell proliferation was modelled directly on the macroscopic level by way of some growth term, mostly of logistic type. While [19] included proliferation based on the "go-or-grow" dichotomy, the approach at hand offers an alternative to this sometimes contested assumption (see e.g., [14, 22, 41, 50]) and considers instead cell-tissue interactions (via cell surface receptors binding to the tissue fibers) as initiators of the cell division process. These interactions described in (5) feature a growth function μ depending on the macroscopic cell density, position, and cell velocity, together with a function χ characterizing the innovations of subcellular dynamics according to the cell-tissue interactions. The new model involves a kinetic transport equation for the glioma cell density on the mesoscale and an ODE for the binding of cell surface receptors to the tissue fibers on the microscale. This two-scale model is globally well posed, by the theory in [38]. A parabolic scaling argument leads to an effective equation for the tumor cell density on the macroscale, for which the (local) well posedness is proved. The occurring coefficients (tumor diffusion tensor, tumor drift velocity, and the transport velocity in the supplementary first order term carrying the information from the subcellular level) can be explicitly determined with respect to the directional distribution q of tissue fibers and the volume fraction Q of brain matter and computed/estimated from DTI data. The simulation results are in accordance with previous findings [18, 19] that glioma follow white matter tracts, hence leading to the clinically observed finger-like structures [13, 16, 23, 40]. Comparisons with pure diffusion or monoscale models show that those predict a more compact shape of the tumor, thereby underestimating its degree of extent in the direction of white matter tracts. Compared to our previous model in [19] describing cell proliferation via "go-or-growth", the current setting predicts enhanced glioma invasion and growth. To decide which of these models better reproduces the actual tumor behavior remains a future task, as patient data are needed. [7]

There are still several interesting issues to be addressed in connection with this modeling approach. In (5) we assumed for simplicity that the growth function μ was independent on the subcellular dynamics and later on we even dropped the dependence on the cell velocity. These dependencies seem to be biologically related, as the distribution and number of a a cell's surface receptors bound to the tissue fibers is relevant both for its velocity and its internal biochemical activity (including proliferation). Hence, handling one of these issues would implicitly provide some information about the other. This would certainly complicate the deduction of the macroscopic equation in Subsection 3.1 but would possibly lead to different source terms on the right hand side of (19). Again, the best choice of μ and how much of the related information should be accounted for is a matter of data availability.
Therapy modeling is another prominent issue: for instance, the common radiotherapy methods involve simple statistics in connection with the survival ability of the irradiated tissue. However, such approaches cannot provide a satisfactory description of the therapy effects on the cell dynamics (recovery of the damaged cells, proliferation, sensitivity against treatment etc.), hence the need of cell population models

[7] so far only DTI data for the brain structure of a healthy subject were available for our simulations

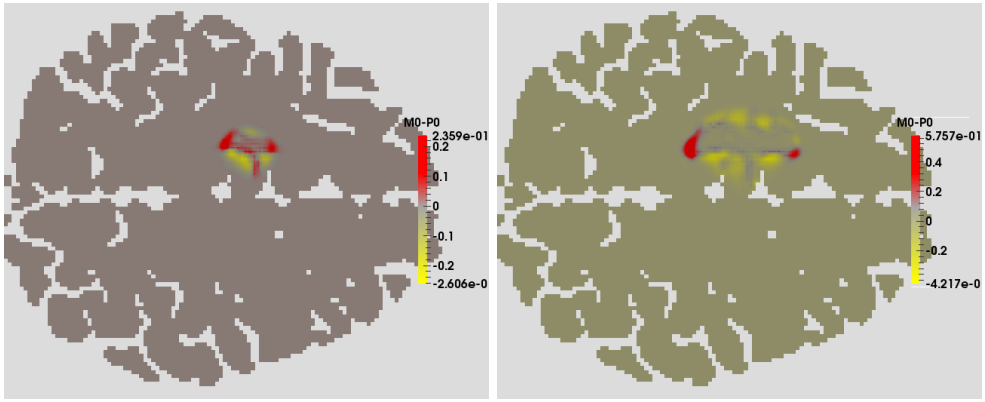

(a) Day 280, $\kappa = 10$ (b) Day 560, $\kappa = 10$

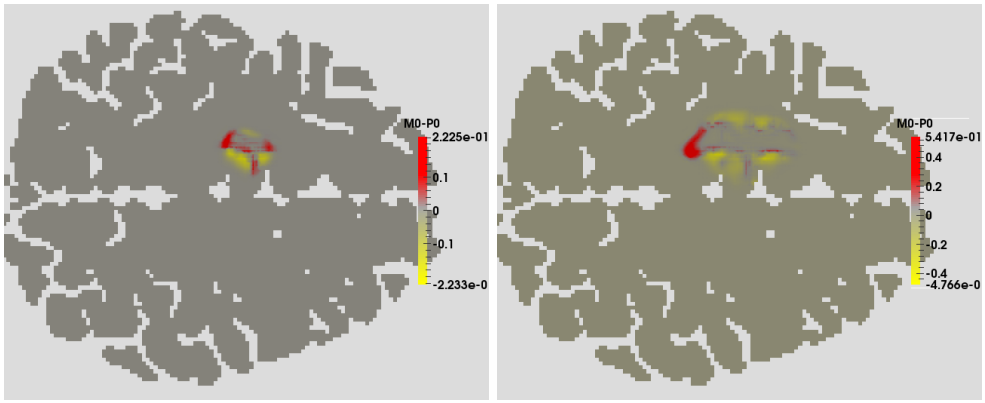

(c) Day 280, $\kappa = 20$ (d) Day 560, $\kappa = 20$

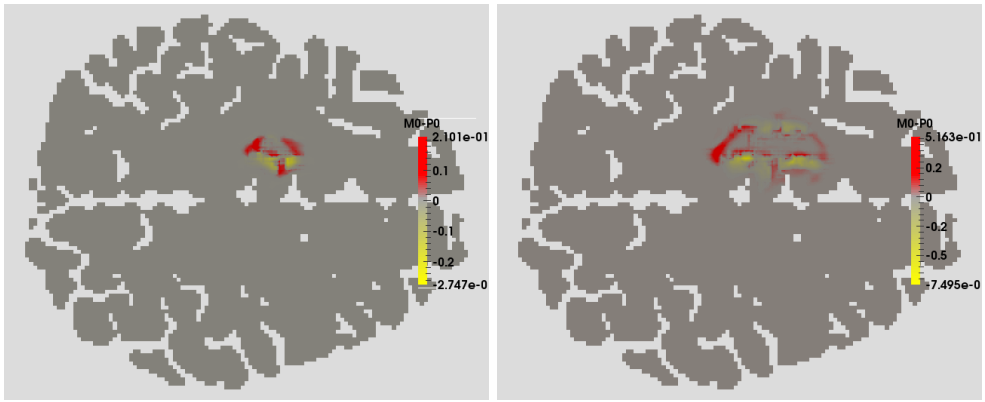

(e) Day 280, $\kappa = 10000$ (f) Day 560, $\kappa = 10000$

Figure 7: Difference $M_0 - P_0$ between the solutions obtained by our multiscale approach and the one using a pure mesoscopic model leading to a macroscale equation with fully anisotropic diffusion, respectively.

characterizing the behavior of tumor and tissue by way of differential equations or in the framework of hybrid discrete/continuous settings. Mathematical models and their simulations can offer an advantageous platform for investigating the effects, but also the combinations of different types of therapy (surgery, chemo and radiotherapy) and their scheduling. Thereby, it is desirable to have performant models to predict the spatial tumor extent over time. Extending our multiscale approach to include therapy issues is ongoing work.

Aknowledgements

We thank Carsten Wolters (Institute of Biomagnetism and Biosignal Analysis, University of Münster) for the preprocessesd DTI data and Katarina Wolf (Radboud University Nijmegen) for very interesting

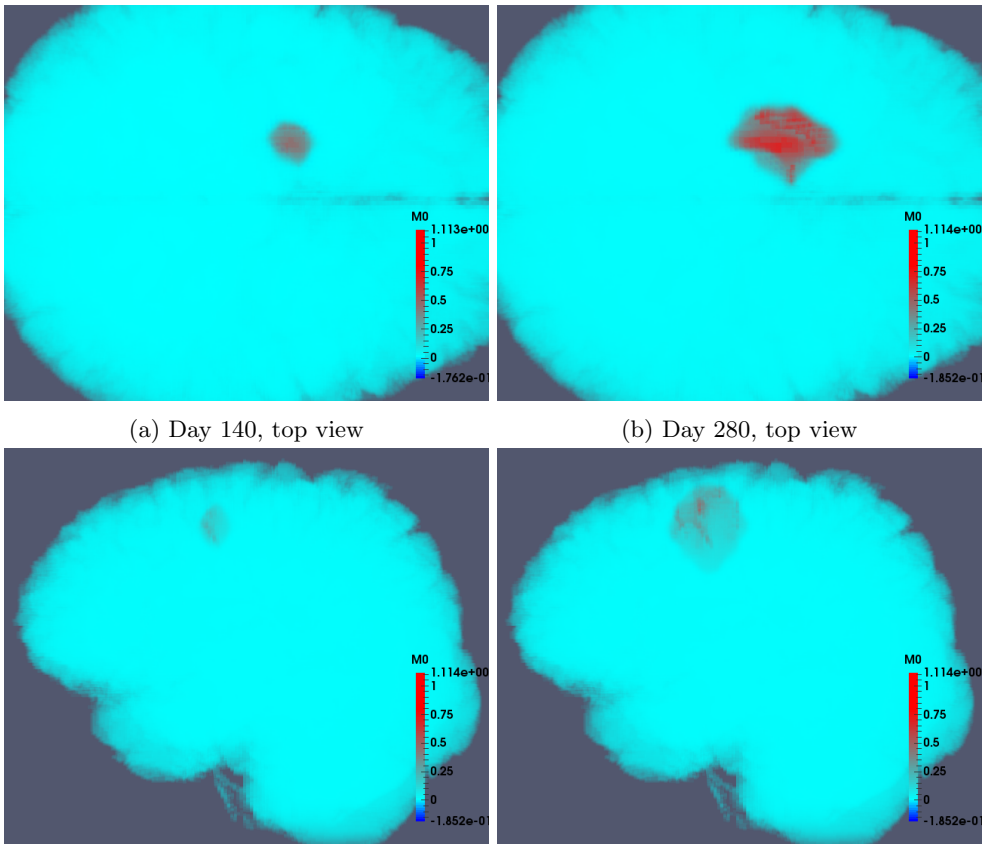

(a) Day 140, top view (b) Day 280, top view

(c) Day 140, side view (d) Day 280, side view

Figure 8: 3D Simulations of (19).

discussions about cell motility and related data allowing us to assess some of the parameters involved in the model.

References

[1] J.A. Aguirre-Ghiso. Models, mechanisms, and clinical evidence for cancer dormancy. 7:834–846, 2007.

[2] Z. Bajzer, S. Vuk-Pavlovic, and M. Huzak. Mathematical modeling of tumor growth kinetics. In J.A. Adam and N. Bellomo, editors, *A Survey of Models for Tumor-Immune System Dynamics*, pages 89–134. Birkhäuser, Boston, 1997.

[3] P. Basser. Diffusion and diffusion tensor MR imaging:fundamentals. In S.W. Atlas, editor, *Magnetic Resonance Imaging of the Brain and Spine*, pages 1752–1767. Lippincott Williams, Philadelphia, 2008.

[4] P. Bastian, M. Blatt, A. Dedner, C. Engwer, R. Klöfkorn, R. Kornhuber, M. Ohlberger, and O. Sander. A generic grid interface for parallel and adaptive scientific computing. Part II: Implementation and tests in DUNE. *Computing*, 82(2–3):121–138, 2008.

[5] A.M. Belkin, G. Tsurupa, E. Zemskov, Y. Veklich, J.W. Weisel, and L. Medved. Transglutaminase-mediated oligomerization of the fibrin(ogen) αC domains promotes integrin-dependent cell adhesion and signaling. *Blood*, 105(9):3561–3568, 2005.

[6] N. Bellomo. *Modeling Complex Living Systems. A Kinetic Theory and Stochastic Game Approach.* Birkhäuser, 2008.

[7] N. Bellomo, A. Bellouquid, J. Nieto, and J. Soler. Complexity and mathematical tools toward the modeling of multicellular growing systems. *Mathematical and Computer Modelling*, 51:441–451, 2010.

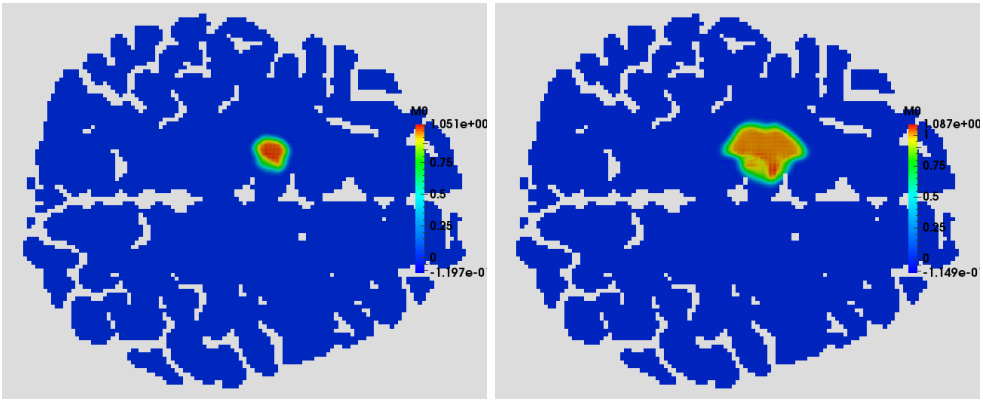

Day 140 Day 280

(a) 2D simulation of (19) using fractional anisotropy and μ_1

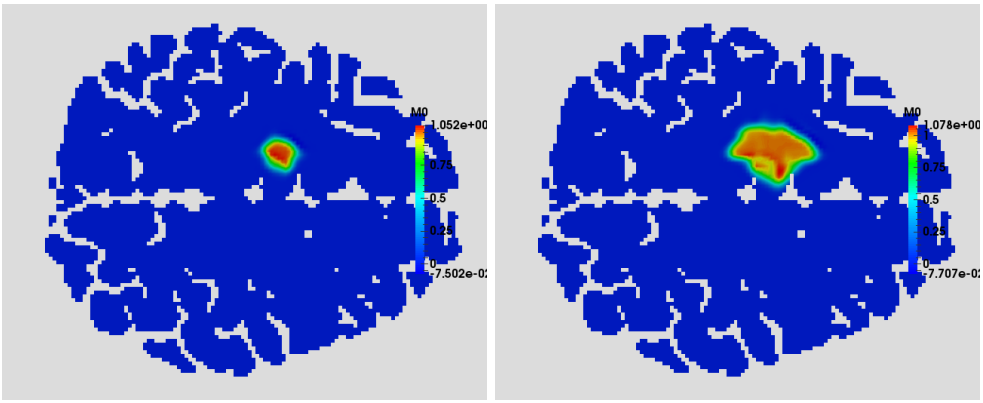

Day 140 Day 280

(b) Projected 3D simulation of (19) using fractional anisotropy and μ_1

Figure 9: 2D and projected 3D simulations of (19)

[8] M.E. Berens and A. Giese. What's malignant about astrocytomas? studies of brain tumor proliferation and migration. *Barrows Neurol Inst Quarterly*, 12:1522, 1996.

[9] P.Y. Bondiau, O. Clatz, M. Sermesant, P.Y. Marcy, H. Delignette, M. Frenay, and N. Ayache. Biocomputing: numerical simulation of glioblastoma growth using diffusion tensor imaging. *Physics in Medicine and Biology*, 53:879–893, 2008.

[10] M. R. Chicoine and D. L. Silbergeld. Assessment of brain tumor cell motility in vivo and in vitro. *Journal of Neurosurgery*, 82(4):615–622, 1995.

[11] O. Clatz, M. Sermesant, P.Y. Bondiau, H. Delignette, S.K. Warfield, G. Malandain, and N. Ayache. Realistic simulation of the 3D growth of brain tumors in MRI images coupling diffusion with biomechanical deformation. *IEEE Transactions for medical imaging*, 24(10):1334–1346, 2005.

[12] D. Cobzas, P. Mosayebi, A. Murtha, and M. Jagersand. Tumour invasion margin on the Riemannian space of brain fibers. In *International Conference on Medical Image Computing and Computer Assisted Intervention, MICCAI*, 2009.

[13] S. Coons. Anatomy and growth patterns of diffuse gliomas. In M. Berger and C. Wilson, editors, *The gliomas*, pages 210–225. W.B. Saunders Company, Philadelphia, 1999.

[14] A. Corcoran and R.F. Del Maestro. Testing the "go or grow" hypothesis in human medulloblastoma cell lines in two and three dimensions. *Neurosurgery*, 53:174–185, 2003.

[15] G. D'Abaco and A. Kaye. Integrins: Molecular determinants of glioma invasion. *J. of Clinical Neurosci.*, 14:1041–1048, 2007.

[16] C. Daumas-Duport, P. Varlet, M.L. Tucker, F. Beuvon, P. Cervera, and J.P. Chodkiewicz. Oligodendrogliomas. part i: Patterns of growth, histological diagnosis, clinical and imaging correlations: A study of 153 cases. *Journal of Neuro-Oncology*, 34:37–59, 1997.

[17] M. Descoteaux. *High Angular Resolution Diffusion MRI: from Local Estimation to Segmentation and Tractography.* Ph.D. thesis, Université Nice-Sophia Antipolis, 2008.

[18] C. Engwer, T. Hillen, M. Knappitsch, and C. Surulescu. Glioma follow white matter tracts; a multiscale DTI-based model. *J. of Math. Biol.*, 2014.

[19] C. Engwer, M. Knappitsch, and C. Surulescu. A multiscale model for glioma spread including cell-tissue interactions and proliferation. *preprint, WWU Münster*, 2014.

[20] A. Ern, A. F. Stephansen, and P. Zunino. A discontinuous galerkin method with weighted averages for advection–diffusion equations with locally small and anisotropic diffusivity. *IMA Journal of Numerical Analysis*, 29(2):235–256, 2009.

[21] P. Friedel and E.B. Broecker. The biology of cell locomotion within three-dimensional extracellular matrix. *Cellular and Molecular Life Sciences*, 57:41–64, 2000.

[22] T. Garay, E. Juhasz, E. Molnar, M. Eisenbauer, A. Czirok, B. Dekan, V. Laszlo, M.A. Hoda, B. Döme, J. Timar, W. Klepetko, W. Berger, and B. Hegedus. Cell migration or cytokinesis and proliferation? revisiting the go or grow hypothesis in cancer cells in vitro. *Exp. Cell Res.*, 319:3094–3103, 2013.

[23] E.R. Gerstner, P.-J. Chen, P.Y. Wen, R.K. Jain, T.T. Batchelor, and G. Sorensen. Infiltrative patterns of glioblastoma spread detected via diffusion MRI after treatment with cediranib. *Neuro-Oncology*, 12(5):466–472, 2010.

[24] A. Giese, L. Kluwe, Meissner H., Michael E., and M. Westphal. Migration of human glioma cells on myelin. *Neurosurgery*, 38:755–764, 1996.

[25] A. Giese and M. Westphal. Glioma invasion in the central nervous system. *Neurosurgery*, 39:235–252, 1996.

[26] D. Hanahan and R.A. Weinberg. Hallmarks of cancer: the next generation. *Cell*, 144(5):646–674, 2011.

[27] T. Hillen and H. Othmer. The diffusion limit of transport equations derived from velocity jump processes. *SIAM Journal on Applied Mathematics*, 61(3):751–775, 2000.

[28] T. Hillen and K.J. Painter. Transport and anisotropic diffusion models for movement in oriented habitats. In M. Lewis, P. Maini, and S. Petrovskii, editors, *Dispersal, Individual Movement and Spatial Ecology*, volume 2071 of *Lecture Notes in Mathematics*, page 46. Springer, 2013.

[29] K.S. Hoek, O.M. Eichhoff, N.C. Schlegel, U. Döbbeling, S. Hemmi, and R. Dummer. In vivo switching of human melanoma cells between proliferative and invasive states. *Cancer Res.*, 68:650–656, 2008.

[30] J.D. Hood and D.A. Cheresh. Role of integrins in cell invasion and migration. *Nature Rev. Cancer*, 2:91–100, 2002.

[31] T. Hoshino, C.B. Wilson, M.L. Rosenblum, and M. Barker. Chemotherapeutic implications of growth fraction and cell cycle time in glioblastomas. *J. Neurosurg.*, 43(2):127–35, 1975.

[32] A. Huttenlocher and A.R. Horwitz. Integrins in cell migration. *Cold Spring Harbour Perspectives in Biology*, 3:1–16, 2011.

[33] A. Jbabdi, E. Mandonnet, H. Duffau, L. Capelle, K.R. Swanson, M. Pelegrini-Issac, R. Guillevin, and H. Benali. Simulation of anisotropic growth of low-grade gliomas using diffusion tensor imaging. *Mang. Res. Med.*, 54:616–624, 2005.

[34] J. Kelkel and C. Surulescu. A multiscale approach to cell migration in tissue networks. *Mathematical Models and Methods in Applied Sciences*, 23(3), 2012.

[35] E. Konukoglu, O. Clatz, P.Y. Bondiau, H. Delignette, and N. Ayache. Extrapolation glioma invasion margin in brain magnetic resonance images: Suggesting new irradiation margins. *Medical Image Analysis*, 14:111–125, 2010.

[36] D.A. Lauffenburger and J.L. Lindermann. *Receptors. Models for binding, trafficing and signaling.* Oxford University Press, 1993.

[37] K.R. Legate, S.A. Wickström, and R. Fässler. Genetic and cell biological analysis of integrin outside-in signaling. *Genes Dev.*, 23:397–418, 2009.

[38] T. Lorenz and C. Surulescu. On a class of multiscale cancer cell migration models: Well-posedness in less regular function spaces. *Math. Models Meth. Appl. Sci.*, 24, 2014. 54 pages.

[39] K.V. Mardia and P.E. Jupp. *Directional Statistics.* Wiley, 1999.

[40] Y. Matsukado, C. MacCarty, and et al.. Kernohan, J. The growth of glioblastoma multiforme (astrocytomas, grades 3 and 4) in neurosurgical practice. *Journal of Neurosurgery*, 18:636–644, 1961.

[41] R.-H. Mattern, S.B. Read, M.D. Pierschbacher, C.-I Sze, B.P. Eliceri, and C.A. Kruse. Glioma cell integrin expression and their interactions with integrin antagonists. *Cancer Ther.*, 3A:325–340, 2005.

[42] K.J. Painter and T. Hillen. Mathematical modelling of glioma growth: the use of diffusion tensor imaging (DTI) data to predict the anisotropic pathways of cancer invasion. *Journal for Theoretical Biology*, 323:25–39, 2013.

[43] M. Ruzicka. *Nichtlineare Funktionalanalysis. Eine Einführung.* Springer, 2004.

[44] R.E. Showalter. *Monotone Operators in Banach Space and Nonlinear Partial Differential Equations.* AMS, 1997.

[45] M. Sidani, D. Wessels, G. Mouneimne, M. Ghosh, S. Goswami, C. Sarmiento, W. Wang, S. Kuhl, M. El-Sibai, J.M. Backer, R. Eddy, D. Soll, and J. Condeelis. Cofilin determines the migration behavior and turning frequency of metastatic cancer cells. *The Journal of Cell Biology*, 179(4):777–791, 2007.

[46] P.C. Sundgren, Q. Dong, D. Gomez-Hassan, S.K. Mukherji, P. Maly, and R. Welsh. Diffusion tensor imaging of the brain: review of clinical applications. *Neurocarciology*, 46:339–350, 2004.

[47] K.R. Swanson, C. Bridge, J.D. Murray, and E.C. Alvord Jr. Virtual and real brain tumors: using mathematical modeling to quantify glioma growth and invasion. *J. Neurol. Sci.*, 216:1–10, 2003.

[48] D.S. Tuch. *Diffusion MRI of complex Tissue Structure.* Ph.D. thesis, University of Chicago, 1996.

[49] J.H. Uhm, C.L. Gladson, and J.S. Rao. The role of integrins in the malignant phenotype of gliomas. *Frontiers in Bioscience*, 4:188–199, 1999.

[50] T.A. Ulrich, E.M. de Juan Pardo, and S. Kumar. The mechanical rigidity of the extracellular matrix regulates the structure, motility, and proliferation of glioma cells. *Cancer Res.*, 69:4167–4174, 2009.

[51] C.H. Wang, J.K. Rockhill, M. Mrugala, D.L. Peacock, A. Lai, K. Jusenius, J.M. Wardlaw, T. Cloughesy, A.M. Spence, R. Rockne, E.C. Alvord Jr., and K.R. Swanson. Prognostic significance of growth kinetics in newly diagnosed glioblastomas revealed by combining serial imaging with a novel biomathematical model. *Cancer Res.*, 69:9133–9140, 2009.